Combined Approach of NMR and Molecular Dynamics within a Biphasic Membrane Mimetic: Conformation and Orientation of the Bradykinin Antagonist Hoe 140

Wolfgang Guba,[†] Rainer Haessner,[†] Gerd Breipohl,[‡] Stefan Henke,[‡] Jochen Knolle,[‡] Vincenzo Santagada,[§] and Horst Kessler*,[†]

Contribution from the Institut für Organische Chemie und Biochemie, Technische Universität München, Lichtenbergstrasse 4, D-85747 Garching, Germany, Hoechst Aktiengesellschaft, General Pharma Research, Peptide and Nucleotide Section, D-65926 Frankfurt am Main, Germany, and Dipartimento Di Chimica Farmaceutica E Tossicologica, Facolti Di Pharmacia, Via De Montegano 19, I-80131 Napoli, Italy

Received February 9, 1994[⊛]

Abstract: The conformation of the highly potent bradykinin antagonist Hoe 140 (D-Arg[0]-Arg[1]-Pro[2]-Hyp[3]-Gly[4]-Thi[5]-Ser[6]-D-Tic[7]-Oic[8]-Arg[9]) in a membrane-like surrounding was determined via NMR spectroscopy in SDS micelles and restrained molecular dynamics (MD) simulations in the novel biphasic membrane mimetic H_2O/CCl_4. The conformation is characterized by a βII′-turn and a βII-turn comprising residues 6–9 and 2–5, respectively, with the three arginine side chains anchored in the water phase and the rest of the molecule positioned in the hydrophobic phase. Selective solvation of the hydroxylated amino acids Hyp[3] and Ser[6] was examined by radial distribution functions, and both the orientation and the dynamics at the interface were analyzed by calculating the time course and the probability distribution of diagnostic atoms relative to the density profile of H_2O/CCl_4. Additional simulations were performed with all ionizable groups treated as charged to demonstrate the unfolding in pure H_2O and the reorientation of Hoe 140 in the biphasic system after completely embedding the refined conformation in the apolar phase.

Introduction

The interaction between peptide hormones and their receptors may be catalyzed by membranes.[1,2] The membrane-bound pathway for receptor recognition and binding implies the accumulation and orientation of the peptide on the membrane surface, thus enhancing the local concentration and reducing the degrees of translational and rotational freedom.[3] This accumulation and preorientation has been furthermore proposed to lower the energy barrier for inducing the bioactive conformation from a *random coil* "structure" usually adopted by unrestrained peptides in the extracellular aqueous phase.[4,5]

As implied above, the rational drug design of membrane-active peptides is closely related to the characterization of the conformation and orientation in the native environment. To our knowledge, there have been no direct experimental investigations simultaneously elucidating the orientation of the peptide at the interface boundary, the depth of intrusion into the bilayer, and the conformational preferences.

To tackle this problem from a pragmatic point of view, Schwyzer introduced the amphiphilic moment[3] as an important new parameter for determining quantitative structure–activity relationships (QSAR) in receptor selection and biological potency. On the theoretical side, explicit membrane-water interfaces were developed[6-10] which, however, require an enormous amount of computer resources. As reported previously,[2,11] we designed a biphasic H_2O/CCl_4 stimulation cell for use in molecular dynamics simulations to mimic the lipophilic and hydrophobic portions of membrane-like systems. This system has the advantage of allowing simulations on common workstations within a reasonable time span and retaining full flexibility of the solute.

Here, we present our results on the highly potent bradykinin (Arg[1]-Pro[2]-Pro[3]-Gly[4]-Phe[5]-Ser[6]-Pro[7]-Phe[8]-Arg[9]) antagonist Hoe 140[12-14] (D-Arg[0]-Arg[1]-Pro[2]-Hyp[3]-Gly[4]-Thi[5]-Ser[6]-D-Tic[7]-Oic[8]-Arg[9]; Hyp, hydroxyproline; Thi, thiophene-yl-alanine; Tic, 1,2,3,4-tetrahydroisoquinoline-3-carboxylic acid; Oic, (3a,*S*,7a*S*)-octahydroindole-2-carboxylic acid), which was investigated in water and SDS micelles by NMR spectroscopy.

It is well-known that linear peptides up to about 20 residues do not form definite secondary structure elements in isotropic media unless stabilized by specific sequences[15,16] or a high content

* To whom correspondence should be addressed.
† Technische Universität München.
‡ General Pharma Research.
§ Via De Montegano 19.
⊛ Abstract published in *Advance ACS Abstracts*, July 15, 1994.

(1) Romano, R.; Dufresne, M.; Prost, M.-C.; Bali, J.-P.; Bayerl, T. M.; Moroder, L. *Biochim. Biophys. Acta* **1993**, *1145*, 235–242.
(2) Moroder, L.; Romano, R.; Guba, W.; Mierke, D. F.; Kessler, H.; Delporte, C.; Winand, J.; Christophe, J. *Biochemistry* **1993**, *32*, 13551–13559.
(3) (a) Sargent, D. F.; Schwyzer, R. *Proc. Natl. Acad. Sci. U.S.A.* **1986**, *83*, 5774–5778. (b) Schwyzer, R. *Biochemistry* **1986**, *25*, 4281–4286. (c) Schwyzer, R. *Chemtracts: Biochem. Mol. Biol.* **1992**, *3*, 347–379.
(4) Schwyzer, R. In *Natural Products and Biological Activities*; Imura, H., Goto, T., Murachi, T., Nakajima, T., Eds.; Tokyo Press and Elsevier: Tokyo, 1986; pp 197–207.
(5) Schwyzer, R. *Biopolymers* **1991**, *31*, 785–792.
(6) Raghavan, K.; Reddy, M. R.; Berkowitz, M. L. *Langmuir* **1992**, *8*, 233–240.
(7) Damodaran, K. V.; Merz, K. M.; Gaber, B. P. *Biochemistry* **1992**, *31*, 7656–7664.
(8) Damodaran, K. V.; Merz, K. M. *Langmuir* **1993**, *9*, 1179–1183.
(9) Heller, H.; Schaefer, M.; Schulten, K. J. *J. Phys. Chem.* **1993**, *97*, 8343–8360.
(10) Bassolino-Klimas, D.; Alper, H. E.; Stouch, T. R. *Biochemistry* **1993**, *32*, 12624–12637.
(11) Guba, W.; Kessler, H. *J. Phys. Chem.* **1994**, *98*, 23–27.
(12) Hock, F. J.; Wirth, K.; Albus, U.; Linz, W.; Gerhards, H. J.; Wiemer, G.; Henke, S.; Breipohl, G.; König, W.; Knolle, J.; Schölkens, B. A. *Br. J. Pharmacol.* **1991**, *102*, 769–773.
(13) Anagnostopulos, H.; Breipohl, G.; Fehlhaber, H. W.; Henke, S.; Knolle, J.; Schölkens, B. A. EPS 0 370 453, 1988.
(14) Knolle, J.; Breipohl, G.; Henke, S.; Wirth, K.; Schölkens, B. In *Proceedings of the Seventh USSR FRG Symposium on Chemistry of Peptides and Proteins and of the Eighth FRG USSR Symposium on Chemistry of Peptides and Proteins*, Dilizhan, USSR, September 23–30, 1989 and Aachen, FRG, September 29–October 3, 1991; Brandenburg, D., Ivanov, V., Voelter, W., Eds.; Mainz, Aachen, 1993; Vol. 5/6, pp 389–395.
(15) Kessler, H. *Angew. Chem., Ind. Ed. Engl.* **1982**, *21*, 512–523.
(16) Imperiali, B.; Fisher, S. L.; Moats, R. A.; Prins, T. J. *J. Am. Chem. Soc.* **1992**, *114*, 3182–3188.

0002-7863/94/1516-7532$04.50/0 © 1994 American Chemical Society

of α,α-disubstituted amino acids[17] or by environmental effects such as the solvent trifluoroethanol[18] or cryomixtures[19] (DMSO–water at low temperatures). Only some indications for a beginning of folding can be found in special peptides,[20] i.e. a higher population of certain folded structures in the conformational equilibrium. As has been pioneered by Wüthrich's group, micelles may induce structures in oligopeptides.[21] The incorporation of peptides into membranes causes drastic line broadening of their NMR signals, which makes it difficult to obtain high-resolution spectra. Further problems are imposed by the high concentration of the lipid in comparison to the embedded peptide and by signal overlap between the membrane forming agent and the solute. Therefore, only few conformational analyses of membrane-bound peptides,[22] employing the method of transferred nuclear Overhauser effects (TRNOE)[23,24] and, in addition to that, orientational analysis of peptides via solid-state NMR,[25-27] have been reported. In order to mimic a membrane-like environment and to improve the relaxation behavior, numerous studies have been performed in micelles.[28]

Preliminary NMR measurements of Hoe 140 in H_2O and D_2O as well as in DMSO showed that this molecule is highly flexible (*random coil*) according to similar NH chemical shifts, chemical shifts close to usual *random coil* values,[29] small splittings of diastereotopic groups, and the lack of long-range NOEs. However, when Hoe 140 is dissolved in deuterated SDS micelles, not only does the spectrum exhibit line broadening, indicating the interaction of Hoe 140 with the micelles by its much longer correlation time τ_c, but strong negative NOEs are also observed. On the basis of the data in SDS micelles, a conformational and orientational analysis of Hoe 140 was performed via restrained MD simulations *in vacuo* and in the newly developed biphasic H_2O/CCl_4 simulation cell[11] assuming one preferred conformation. Additional simulations were performed with all ionizable groups treated as charged to demonstrate the unfolding in pure H_2O and the reorientation of Hoe 140 in the biphasic system after completely embedding the refined conformation in the apolar phase.

The peptide hormone bradykinin (BK) and related kinins display a variety of physiological activities.[30] BK influences vascular tone and permeability, decreases blood pressure, initiates or enhances the release of mediators from leukocytes, and stimulates the nociceptive afferent nerve terminals. Evidence supporting the participation of BK in inflammatory processes,[31] allergic reactions, asthma, and atropic dermatitis emerged only during recent years. BK is also tentatively associated with symptoms of the common cold.[32,33] Specific and potent BK antagonists are, therefore, considered to be a new therapeutic principle for the treatment of diseases with pathologically elevated BK levels. The antagonistic effect is discussed to be connected with a C-terminal β-turn,[28e,34] although recently a β-turn comprising residues 2–5 has been suggested as well.[35] The bradykinin antagonist Hoe 140,[12] now in extended clinical trials, is effective, in intravenous doses of 0.01–1 mg/kg (body weight), in inhibiting the carrageenin-induced rat oedema, a condition that is presumed dependent on endogenous kinins. Hoe 140 is equally potent when administered subcutaneously, where the effect of 1 mg/kg (body weight) lasted for more than 6 h. On the basis of its high potency and long duration of action, Hoe 140 can be expected to effectively antagonize the effects of endogenously generated BK in disease. As such, Hoe 140 is appropriate to evaluate the role of BK in physiology and pathophysiology and to determine the usefulness of BK-antagonism as a novel therapeutic approach in selected disease states.

Methods

NMR Spectroscopy. NMR experiments were performed with a solution of 4 mM Hoe 140 in (a) H_2O, containing 10% D_2O, and (b) D_2O. The pH was adjusted to 4.8 by adding CD_3COOH. The D_2O sample was first lyophilized twice from D_2O and then dissolved in D_2O. Both samples were 320 mM in deuterated SDS, well above the critical micelle concentration of 8.2 mM.[36] 1D-proton spectra were recorded at different temperatures in a range from 300 to 340 K. Proton and carbon spectra were recorded on a Bruker AMX 500 spectrometer and processed on a Bruker X32 workstation using the UXNMR program.

Chemical shifts were calibrated with respect to internal HOD (assuming a chemical shift of 4.67 ppm at 300 K). Water suppression (only for sample a) was achieved using 1.5 s of weak presaturation before the scan and additional presaturation within the whole mixing time for NOESY,[37,38] a 2.5-s weak presaturation pulse for 1D, and a 1.5-s presaturation pulse

(17) Yijayakumar, E. K. S.; Balaram, P. *Biopolymers* **1983**, *22*, 2133–2140.
(18) Mierke, D. F.; Dürr, H.; Kessler, H.; Jung, G. *Eur. J. Biochem.* **1992**, *206*, 39–48.
(19) Temussi, P. A.; Picone, D.; Saviano, G.; Amodeo, P.; Motta, A.; Tancredi, T.; Salvadori, S.; Tomatis, R. *Biopolymers* **1992**, *32*, 367–372.
(20) Dyson, H. J.; Rance, M.; Houghten, R. A.; Lerner, R. A.; Wright, P. E. *J. Mol. Biol.* **1988**, *201*, 161–200.
(21) (a) Lee, K. H.; Fitton, J. E.; Wüthrich, K. *Biochim. Biophys. Acta* **1987**, *911*, 144–153. (b) Bösch, C.; Brown, L. R.; Wüthrich, K. *Biochim. Biophys. Acta* **1980**, *6*-3, 298–312.
(22) (a) Wakamatsu, K.; Okada, A.; Miyazawa, T.; Ohya, M.; Higashijima, T. *Biochemistry* **1992**, *31*, 5654–5660. (b) Gounarides, J. S.; Broido, M. S.; Becker, J. M.; Naider, F. R. *Biochemistry* **1993**, *32*, 908–917.
(23) Clore, G. M.; Gronenborn, A. M. *J. Magn. Reson.* **1982**, *48*, 402–417.
(24) Clore, G. M.; Gronenborn, A. M. *J. Magn. Reson.* **1983**, *53*, 423–442.
(25) Shon, K.-J.; Kim, Y.; Colnago, L. A.; Opella, S. J. *Science* **1991**, *252*, 1303–1305.
(26) Hing, A. W.; Schaefer, J. *Biochemistry* **1993**, *32*, 7593–7604.
(27) Ketchem, R. R.; Hu, W.; Cross, T. A. *Science* **1993**, *261*, 1457–1460.
(28) (a) Olejniczak, E. T.; Gampe, R. T.; Rockway, T. W.; Fesik, S. W. *Biochemistry* **1988**, *27*, 7124–7131. (b) Inagaki, F.; Shimada, I.; Kawaguchi, K.; Hirano, M.; Terawasa, I.; Ikura, T.; Go, N. *Biochemistry* **1989**, *28*, 5985–5991. (c) Cann, J. R.; Vavrek, R. J.; Stewart, J. M.; Mueller, D. D. *J. Am. Chem. Soc.* **1990**, *112*, 1357–1364. (d) Mammi, S.; Peggion, E. *Biochemistry* **1990**, *29*, 5265–69. (e) Lee, S. C.; Russell, A. F.; Laidig, W. D. *Int. J. Peptide Protein Res.* **1990**, *35*, 367–377. (f) Deber, C. M.; Glibowicka, M.; Woolley, G. A. *Biopolymers* **1990**, *29*, 149–157. (g) Karslake, C.; Piotto, M. E.; Pak, Y. K.; Weiner, H.; Gorenstein, D. G. *Biochemistry* **1990**, *29*, 9872–9878. (h) Zetta, C.; Consonni, R.; De Marco, A.; Longhi, R.; Manera, E.; Vecchio, G. *Biopolymers* **1990**, *30*, 899–909. (i) Xu, G.-Y.; Deber, C. M. *Int. J. Peptide Protein Res.* **1991**, *37*, 528–535. (j) Kohda, D.; Inagaki, F. *Biochemistry* **1992**, *31*, 677–685. (k) Hicks, R. P.; Beard, D. J.; Young, J. K. *Biopolymers* **1992**, *32*, 85–96. (l) Henry, G. D.; Sykes, B. D. *Biochemistry* **1992**, *31*, 5284–5297. (m) Malikayil, J. A.; Edwards, J. V.; McLean, L. R. *Biochemistry* **1992**, *31*, 7043–7049. (n) Peters, A. R.; Dekker, N.; van den Berg, L.; Boelens, R.; Kaptein, R.; Slotboom, A. J.; de Haas, G. H. *Biochemistry* **1992**, *31*, 10024–10030. (o) Bruch, M. D.; Rizo, J.; Gierasch, L. M. *Biopolymers* **1992**, *32*, 1741–1754. (p) Graham, W. H.; Carter, E. S., II; Hicks, R. P. *Biopolymers* **1992**, *32*, 1755–1764. (q) Macquaire, F.; Baleux, F.; Huynh-Dinh, T.; Rouge, D.; Neumann, J.-M.; Sanson, A. *Biochemistry* **1993**, *32*, 7244–7254. (r) van de Ven, F. J. M.; van Os, J. W. M.; Aelen, J. M. A.; Wymenga, S. S.; Remerowski, M. L.; Konings, R. N. H.; Hilbers, C. W. *Biochemistry* **1993**, *32*, 8322–8328. (s) Kallick, D. *J. Am. Chem. Soc.* **1993**, *115*, 9317–9318. (t) Tessari, M.; Foffani, M. T.; Mammi, S.; Peggion, E. *Biopolymers* **1993**, *33*, 1877–1887.
(29) Wüthrich, K. *NMR of Proteins and Nucleic Acids*; Wiley: New York, 1986.
(30) Regoli, D.; Barabe, J. C. *Pharmacol. Rev.* **1980**, *32*, 1–46.
(31) Farmer, S. G.; Burch, R. M. In *Bradykinin Antagonists. Basic and Clinical Research*; Burch, R. M., Ed.; Marcel Dekker: New York, 1991; pp 1–31.
(32) Proud, D.; Reynolds, C. J.; Lacapra, S.; Schotka, A.; Lichtenstein, L. M.; Naclerio, R. M. *Am. Rev. Respir. Dis.* **1988**, *137*, 613–616.
(33) Naclerio, R. M.; Proud, D.; Lichtenstein, L. M.; Sobotka-Kagey, A.; Hemdley, J. O.; Sorrentino, J.; Gwaltney, J. M. *J. Infect. Dis.* **1988**, *157*, 133–142.
(34) (a) Kyle, D. J.; Martin, J. A.; Farmer, S. G.; Burch, R. M. *J. Med. Chem.* **1991**, *34*, 1230–1233. (b) Kyle, D. J.; Blake, P. R.; Hicks, R. P.; Klimbowski, V. J. In *Bradykinin Antagonists. Basic and Clinical Research*; Burch, R. M., Ed.; Marcel Dekker: New York, 1991; pp 131–146. (c) Kyle, D. J.; Martin, J. A.; Burch, R. M.; Carter, J. P.; Lu, S.; Meeker, S.; Prosser, J. C.; Sullivan, J. P.; Togo, J.; Noronha-Blob, L.; Sinsko, J. A.; Walters, R. F.; Whaley, L. W.; Hiner, R. N. *J. Med. Chem.* **1991**, *34*, 2649–2653. (d) Kyle, D. J.; Green, L. M.; Blake, P. R.; Smithwick, D.; Summers, M. F. *Peptide Res.* **1992**, *5*, 206–209. (e) Kyle, D. J.; Blake, P. R.; Smithwick, D.; Green, L. M.; Martin, J. A.; Sinsko, J. A.; Summers, M. F. *J. Med. Chem.* **1993**, *36*, 1450–1460.
(35) Liu, X.; Stewart, J. M.; Gera, L.; Kotovych, G. *Biopolymers* **1993**, *33*, 1237–1247.
(36) Mukerjee, P.; Mysels, K. J. *Critical Micelle Concentrations in Aqueous Surfactant Systems*, National Bureau of Standards, NSRDS-NBS 36, Washington, 1971.
(37) Jeener, J.; Meier, B. H.; Bachmann, P.; Ernst, R. R. *J. Chem. Phys.* **1979**, *71*, 4546–4553.
(38) Kumar, A.; Ernst, R. R.; Wüthrich, K. *Biochem. Biophys. Res. Commun.* **1980**, *95*, 1–6.

Table 1. Proton Chemical Shifts,[a] Coupling Constants,[b] and NH Temperature Coefficients[c] for Hoe 140 in SDS-Micelles in Aqueous Solution

peptide residue	NH	α	β	γ	other protons	J (Hz)	ΔT (-ppb/K)
D-Arg^0		4.05	1.71, 1.91	1.68[d]	δ, 3.16;[d] εNH, 7.16		
Arg^1	8.62	4.41	1.88[d]	1.73, 1.98	δ, 3.23, 3.40; εNH, 7.28		5.8
Pro^2		4.73	1.84, 2.35	1.92, 1.98	δ, 3.40, 3.87		
Hyp^3		4.50	2.03, 2.25	4.59	δ, 3.83[d]		
Gly^4	8.65	3.80, 4.02					8.1
Thi^5	7.80	4.78	3.17, 3.46		3, 6.70; 4, 6.66; 5, 6.98	6.7	2.4
Ser^6	8.94	4.81	3.65, 3.74			8.5	9.0
D-Tic^7		4.23	2.80, 2.95		1, 3.30, 4.07; 5, 7.13; 6 and 7, 7.13, 7.17; 8, 7.01		
Oic^8		4.49	2.02, 2.36		3a, 2.42; 4_{pro-R}, 1.85; 4_{pro-S}, 1.43; 5_{pro-R}, 1.36; 5_{pro-S}, 1.43; 6_{pro-R}, 0.98; 6_{pro-S}, 1.66; 7_{pro-R}, 2.04; 7_{pro-S}, 1.43; 7a, 3.72		
Arg^9	7.62	4.16	1.69, 1.91	1.80[d]	δ, 3.15;[d] εNH, 7.08	7.4	4.0

[a] Chemical shifts are reported in ppm relative to HOD at 4.67 ppm downfield from tetramethylsilane. [b] Coupling constants refer to $J_{NH-H\alpha}$ and were measured from 1D spectra. [c] The temperature coefficients of the amide protons are the result of a linear regression analysis from five points between 300 and 340 K. [d] Degenerate diastereotopic protons.

for ROESY. For TOCSY[39] a modification of the basic pulse sequence[40] with the 1-$\bar{1}$ sequence and a homospoil pulse was used (Δ_1-90°(ϕ_1)-t_1-MLEV17-90°(ϕ_2)-HS-Δ_{HS}-90°(ϕ_3)-Δ_{JR}-90°(ϕ_4)-t_2(ϕ_5) with ϕ_1 = 31130220, ϕ_2 = 13312002, ϕ_3 = 0022113322003311, ϕ_4 = 2200331100221133, ϕ_5 = 0022113322003311, Δ_1 = 1.4 s, $\Delta_{HS} \approx 4$ ms, and Δ_{JR} = *dwell time*). For assignment of the spin systems, the DQF-COSY spectrum (only sample b without water suppression) was recorded. NOESY spectra were recorded at 300 K with two different mixing times: 40 and 120 ms. The ROESY[41,42] spectrum with a mixing time of 120 ms was recorded to exclude exchange phenomena for NH-NH cross peaks in the NOESY spectra. DQF-COSY, NOESY, ROESY, and TOCSY spectra were typically recorded with 5263 Hz spectral width in both dimensions and 4096 data points in f2 and 512 data points in f1 with 16 (TOCSY) or 32 (DQF-COSY, NOESY, ROESY) scans at each increment. All 2D experiments were acquired in the phase-sensitive mode by using time-proportional phase incrementation (TPPI). For data processing the matrices were one time zero-filled in f1 and apodized by a squared sine bell function shifted by $\pi/2$ in both dimensions.

For the temperature coefficients five one-dimensional experiments with presaturation were recorded between 300 and 340 K. The complete proton assignment is given in Table 1. Diastereotopic assignment was only possible for the protons bound to carbons 4–7 of Oic[8].

Distances from the NOESY experiment were obtained by the two-spin approximation. The most intense peak between diastereotopic protons was taken as a reference with 1.78 Å. The computed distances (Table 2) were used as input for restrained MD except for the trivial distances between diastereotopic protons, distances including degenerated diastereotopic protons (Arg^0, Arg^1, Arg^9), distances to aromatic protons in Thi[5], and distance to all arginine-εNHs. Only two distances restraints indicate a folding back of the peptide chain: Oic$^8_{H\alpha}$–Gly$^4_{NH}$ = 2.8 Å (Figure 1) and Thi$^5_{NH}$–Gly$^4_{NH}$ = 3.2 Å.

Computational Procedure. MD simulations and interactive modeling were performed with DISCOVER (Consistent Valence Force Field) and INSIGHT II from Biosym Technologies of San Diego, CA, on SGI 240/GT, Crimson, and Cray YMP computers. Because of the lack of Lennard-Jones parameters for sulfur in thiophene, thienylalanine (Thi) was replaced with the isoelectronic phenylalanine. The conformation of Hoe 140 was first refined in vacuo for 50 ps at 500 K and further for 150 ps at 300 K employing the NMR-derived distances restraints with a maximum force of 1000 kcal Å^{-1} mol^{-1}. The averaged and energy-minimized molecule was placed into a two-phase (H_2O/CCl_4) simulation cell ($x = z = 25$ Å, $y = 35$ Å; 247 H_2O, 65 CCl_4) using 3-dimensional periodic boundary conditions. The y-axis was the normal to the phase interface. The arginine residues were positioned in the aqueous phase, and the remainder of the molecule was positioned in the hydrophobic phase. As described elsewhere,[11] this simulation cell mimics the lipophilic and hydrophobic portion of membranes and micelles as two media of differing polarity, viscosity, and H-bonding capabilities. Except for CCl_4, treated as one atom, all atoms were simulated explicitly. The Lennard-Jones parameters for H_2O and CCl_4 and the charges for H_2O were taken from Berendsen[43] and Rebertus,[44] respectively. The geometric mean was used for the parameters between unlike atoms. Neighbor lists for the calculation of nonbonded interactions were updated every 10 fs within a radius of 13 Å. The actual calculation of nonbonded interactions was carried out up to a radius of 11 Å without the use of switching functions. For all the MD simulations a time step of 1 fs was employed. The simulation protocol consisted of two conjugate gradient energy-minimization cycles (first solute was fixed, and then all atoms were allowed to move freely) with a convergence criterion of 1 kcal/Å. The MD phase of the calculation involved gradual heating starting from 10 K and increasing to 50, 100, 150, 200, 250, and finally 300 K in 2-ps steps, each by direct scaling of velocities. After a 20-ps equilibration period with temperature and pressure bath coupling[45] (300 K, 1 bar) configurations were saved every 200 fs for another 50 ps, applying distance restraints with a maximum force of 1000 kcal Å^{-1} mol^{-1}. The averaged structure was energy-minimized with a convergence criterion of 0.001 kcal/Å. The MD simulation was continued without restraints for another 150 ps with the sampling rate unchanged. One iteration of the two-phase simulation took approximately 0.9 s on an SGI Crimson.

Two additional simulations were performed with the average and energy-minimized conformation, one in pure H_2O ($x = y = z = 33$ Å, 1129 H_2O) and the other in H_2O/CCl_4 ($x = z = 3$ Å, $y = 50$ Å; 409 H_2O, 173 CCl_4) with the peptide completely embedded in the apolar phase. All ionizable groups were treated as charged without counterions being included. The neighbor lists for calculation of nonbonded interactions were updated every 10 fs within a radius of 14 Å, and the actual calculation of nonbonded interactions was carried out up to a radius of 12 Å without the use of switching functions. The simulation protocol of the water simulation was as follows. After 2000 steps employing the *steepest descents* and 3000 steps using the *conjugate gradients* algorithm with the solute kept fixed to relax the hydration shell, the complete system was minimized with a convergence criterion of 1 kcal/Å, applying distance restraints with a maximum force of 1000 kcal Å^{-1} mol^{-1}. After the gradual heating period described above, the MD simulation was continued in the NpT-ensemble for 5 ps with restraints (frames were sampled every 500 fs) and for another 45 ps without distance restraints (sampling rate once every 200 fs). One iteration took 1.2 s on a CRAY YMP. The computational procedure for the reorientation of Hoe 140 in H_2O/CCl_4 will be explained in the Results and Discussion.

Results and Discussion

Conformation and Orientation of Hoe 140 in H_2O/CCl_4. The averaged and energy-minimized conformation from the two-phase simulation and the corresponding backbone dihedral angles are depicted in Figure 2 and Table 3, respectively. It can be characterized by a βII′-turn comprising residues 6–9 and a βII-turn between residues 2 and 5. This is in accordance with the

(39) Braunschweiler, L.; Ernst, R. R. *J. Magn. Reson.* **1983**, *53*, 521–528.
(40) Bax, A.; Davis, D. G. *J. Magn. Reson.* **1985**, *65*, 355–360.
(41) Bothner-By, A. A.; Stephens, R. L.; Lee, J.; Warren, C. D.; Jeanloz, R. W. *J. Am. Chem. Soc.* **1984**, *106*, 811–813.
(42) Bax, A.; Davis, D. G. *J. Magn. Reson.* **1985**, *63*, 207–213.
(43) Berendsen, H. J. C.; Postma, J. P. M.; van Gunsteren, W. F.; Hermans, J. In *Intermolecular Forces*; Pullman, B., Ed.; Reidel: Dordrecht, The Netherlands, 1981; pp 331–342.
(44) Rebertus, D. W.; Berne, B. J.; Chandler, D. *J. Chem. Phys.* **1979**, *70*, 3395–3400.
(45) Berendsen, H. J. C.; Postma, J. P. M.; van Gunsteren, W. F.; DiNola, A.; Haak, J. R. *J. Chem. Phys.* **1984**, *81*, 3684–3690.

Table 2. Distances (Å) Calculated from NOESY Spectra of Hoe 140 in H_2O and D_2O

protons involved	distance[a]	protons involved	distance[a]	protons involved	distance[a]
Arg^0_{α}, Arg^1_{NH}	2.2, 2.3	Arg^0_{α}, $Arg^0_{\beta h}$	2.5, 2.6	Arg^0_{α}, $Arg^0_{\beta l}$	2.3, 2.4
Arg^0_{γ}, $Arg^0_{\epsilon NH}$	2.9	Arg^0_{δ}, $Arg^0_{\epsilon NH}$	2.5, 2.6	Arg^1_{NH}, Arg^1_{α}	3.1, 3.5
Arg^1_{α}, $Pro^2_{\delta h}$	2.7, 2.8	Arg^1_{α}, $Pro^2_{\delta l}$	2.2, 2.5	Arg^1_{α}, Arg^1_{β}	2.3
Arg^1_{α}, $Arg^1_{\gamma h}$	2.9, 3.0	Arg^1_{α}, $Arg^1_{\gamma l}$	3.2, 3.5	Arg^1_{β}, $Arg^1_{\delta h}$	2.3, 2.4
Arg^1_{β}, $Arg^1_{\epsilon NH}$	3.1, 3.3	Arg^1_{β}, $Pro^2_{\delta h}$	2.0, 2.1	Arg^1_{β}, $Pro^2_{\delta l}$	2.8, 3.0
$Arg^1_{\gamma h}$, $Pro^2_{\delta h}$	2.6, 2.7	$Arg^1_{\delta h}$, $Arg^1_{\delta l}$	1.9	$Arg^1_{\delta h}$, $Arg^1_{\epsilon NH}$	2.8
Pro^2_{α}, $Pro^2_{\beta h}$	2.7, 2.8	Pro^2_{α}, $Pro^2_{\beta t}$	2.3	Pro^2_{α}, Hyp^3_{δ}	1.8, 1.9
$Pro^2_{\beta h}$, $Pro^2_{\beta l}$	1.9	$Pro^2_{\beta h}$, Hyp^3_{δ}	2.9	$Pro^2_{\beta t}$, Hyp^3_{δ}	2.6, 2.7
$Pro^2_{\delta h}$, $Pro^2_{\delta l}$	1.9, 2.0	Hyp^3_{α}, $Hyp^3_{\beta h}$	2.2, 2.3	Hyp^3_{α}, $Hyp^3_{\beta l}$	2.1
$Hyp^3_{\beta h}$, $Hyp^3_{\beta l}$	1.8, 1.9	$Hyp^3_{\beta h}$, Hyp^3_{γ}	2.2, 2.3	$Hyp^3_{\beta h}$, Hyp^3_{δ}	2.4, 2.6
$Hyp^3_{\beta l}$, Hyp^3_{γ}	2.4, 2.5	$Hyp^3_{\beta l}$, Hyp^3_{δ}	2.8, 3.2	Hyp^3_{γ}, Hyp^3_{δ}	2.0
Gly^4_{NH}, Thi^5_{NH}	3.2	Gly^4_{NH}, $Gly^4_{\alpha h}$	2.6	Gly^4_{NH}, Oic^8_{α}	2.7, 2.9
$Gly^4_{\alpha h}$, $Gly^4_{\alpha t}$	1.8, 1.9	$Gly^4_{\alpha h}$, Thi^5_{NH}	3.2, 3.4	$Gly^4_{\alpha l}$, Thi^5_{NH}	3.2
Thi^5_{NH}, $Thi^5_{\beta h}$	2.7	Thi^5_{NH}, $Thi^5_{\beta l}$	2.5	Thi^5_{α}, $Thi^5_{\beta h}$	2.4
Thi^5_{α}, $Thi^5_{\beta t}$	2.7	Thi^5_{α}, Thi^5_{3}	2.7, 2.8	$Thi^5_{\beta h}$, $Thi^5_{\beta l}$	1.9
$Thi^5_{\beta h}$, Thi^5_{3}	3.2, 3.6	$Thi^5_{\beta l}$, Thi^5_{3}	3.1, 3.4	Ser^6_{NH}, $Ser^6_{\beta h}$	3.2, 3.5
Ser^6_{NH}, $Ser^6_{\beta l}$	3.5, 4.4	Ser^6_{NH}, Tic^7_{1h}	3.5, 3.8	Ser^6_{NH}, Tic^7_{1l}	3.5, 4.0
Ser^6_{α}, $Ser^6_{\beta h}$	2.7, 2.8	Ser^6_{α}, $Ser^6_{\beta l}$	2.5	Ser^6_{α}, Tic^7_{1h}	2.5
Ser^6_{α}, Tic^7_{1l}	2.1, 2.2	$Ser^6_{\beta h}$, $Ser^6_{\beta l}$	1.8, 1.9	Tic^7_{α}, $Tic^7_{\beta h}$	2.6, 2.8
Tic^7_{α}, $Tic^7_{\beta l}$	2.5, 2.7	Tic^7_{α}, $Oic^8_{7_{pro\text{-}R}}$	2.5, 2.6	Tic^7_{α}, $Oic^8_{7_{pro\text{-}S}}$	2.9, 3.3
Tic^7_{α}, Oic^8_{7a}	2.1, 2.2	$Tic^7_{\beta h}$, $Tic^7_{\beta t}$	1.9	$Tic^7_{\beta h}$, Tic^7_{5}	2.7, 2.8
$Tic^7_{\beta h}$, Tic^7_{1h}	2.7, 2.8	$Tic^7_{\beta h}$, Oic^8_{7a}	3.0, 3.3	$Tic^7_{\beta l}$, Tic^7_{5}	2.4, 2.5
$Tic^7_{\beta l}$, Oic^8_{7a}	2.6, 2.7	Tic^7_{1l}, Tic^7_{8}	2.4, 2.7	Tic^7_{1h}, Tic^7_{8}	2.7, 3.1
Tic^7_{1h}, Tic^7_{1l}	2.0, 2.1	Oic^8_{α}, Arg^9_{NH}	2.7, 3.4	$Oic^8_{\beta h}$, $Oic^8_{\beta l}$	1.8, 1.9
$Oic^8_{\beta l}$, Arg^9_{NH}	3.5, 3.7	Oic^8_{3a}, $Oic^8_{4_{pro\text{-}R}}$	2.3	Oic^8_{3a}, $Oic^8_{4_{pro\text{-}S}}$	2.3, 2.5
Oic^8_{3a}, Oic^8_{7a}	2.3, 2.6	$Oic^8_{4_{pro\text{-}R}}$, $Oic^8_{4_{pro\text{-}S}}$	1.8, 1.9	$Oic^8_{4_{pro\text{-}R}}$, $Oic^8_{5_{pro\text{-}R}}$	2.2, 2.5
$Oic^8_{4_{pro\text{-}R}}$, $Oic^8_{5_{pro\text{-}S}}$	2.2, 2.5	$Oic^8_{4_{pro\text{-}S}}$, Oic^8_{7a}	2.9, 3.3	$Oic^8_{4_{pro\text{-}S}}$, $Oic^8_{5_{pro\text{-}S}}$	2.3
$Oic^8_{5_{pro\text{-}S}}$, $Oic^8_{6_{pro\text{-}R}}$	2.3	$Oic^8_{5_{pro\text{-}S}}$, $Oic^8_{6_{pro\text{-}S}}$	2.1	$Oic^8_{6_{pro\text{-}R}}$, $Oic^8_{6_{pro\text{-}S}}$	1.9, 2.0
$Oic^8_{6_{pro\text{-}R}}$, $Oic^8_{7_{pro\text{-}R}}$	2.6	$Oic^8_{6_{pro\text{-}R}}$, Oic^8_{7a}	2.7, 3.1	$Oic^8_{6_{pro\text{-}S}}$, $Oic^8_{7_{pro\text{-}R}}$	2.2, 2.4
$Oic^8_{6_{pro\text{-}S}}$, Oic^8_{7a}	3.0, 4.1	$Oic^8_{7_{pro\text{-}R}}$, $Oic^8_{7_{pro\text{-}S}}$	1.8	$Oic^8_{7_{pro\text{-}R}}$, Oic^8_{7a}	2.4, 2.6
$Oic^8_{7_{pro\text{-}R}}$, Arg^9_{NH}	2.8, 3.2	$Oic^8_{7_{pro\text{-}S}}$, Oic^8_{7a}	2.7, 3.0	Arg^9_{NH}, Arg^9_{α}	2.7, 2.9
Arg^9_{NH}, $Arg^9_{\beta h}$	2.7, 2.9	Arg^9_{NH}, $Arg^9_{\beta l}$	3.1, 3.3	Arg^9_{NH}, Arg^9_{γ}	2.7, 2.8
Arg^9_{α}, $Arg^9_{\beta h}$	2.6, 2.7	Arg^9_{α}, $Arg^9_{\beta t}$	2.6, 3.0	Arg^9_{α}, Arg^9_{γ}	2.9, 3.0
$Arg^9_{\beta h}$, $Arg^9_{\epsilon NH}$	3.3, 4.0	$Arg^9_{\beta l}$, $Arg^9_{\epsilon NH}$	3.7	Arg^9_{γ}, $Arg^9_{\epsilon NH}$	2.8, 2.9
Arg^9_{δ}, $Arg^9_{\epsilon NH}$	2.8, 2.9				

[a] Two values are given if NOESY volumes differ either between upper and lower diagonal cross peaks or between the measurements in H_2O/D_2O and pure D_2O.

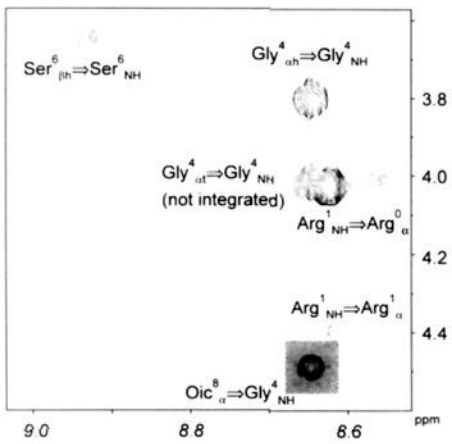

Figure 1. Part of the NOESY spectrum, which shows the cross peaks of most structurally interesting residues (marked by shaded box).

low-temperature coefficients[46] for the amide protons of Thi^5 and Arg^9 (Table 1). However, an unambiguous interpretation of the amide temperature coefficients is not possible, because they might be influenced by the micellar environment. It is also well-known that a D-amino acid in position $i + 1$ induces a βII′-turn[47] and that Pro is often found in position $i + 1$ of a βII-turn.[48,49] The two β-turns are cross-linked by an additional hydrogen bond between the amide hydrogen of Gly^4 and the carbonyl oxygen of D-Tic^7. Furthermore, it is interesting to note that the secondary structure elements were only established in the two-phase simulation and not during the previous *in vacuo* refinement.

The orientation of the molecule in the biphasic environment, averaged over the 150-ps production period, is displayed in Figure 3. The residues in positions $i + 1$ and $i + 2$ of the βII′-turn are deeply buried in the hydrophobic phase, whereas the amino acids in positions i and $i + 3$ are anchored to the aqueous phase via their side chains. The residues of the βII-turn are also situated in a hydrophobic environment. This orientation is stabilized by a hydrogen bond between the hydroxylic group of Hyp^3 and the carbonyl oxygen of Oic^8.

In order to analyze the orientation at the interface, illustrated by the density profile for H_2O/CCl_4, in more detail, the probability distributions and the time course of the y-coordinates of selected atoms relative to the arithmetic center of the water phase are plotted in Figure 4. The density profile was calculated from the complete 150-ps trajectory by counting the number of oxygen (for H_2O) or carbon (for CCl_4) atoms in cross-sections with a thickness of 0.5 Å in the y-direction and normalizing the resulting atomic densities with the idealized atomic densities of H_2O and CCl_4, respectively. The probability distribution shows the average occupancy of cross-sections in the y-direction, whereas the time course of the y-coordinate illustrates the motional dynamics. The following conclusions can be drawn. The arginine side chains tether the molecule to the polar phase (Figure 4a). The residues D-Tic^7 and Oic^8 (βII′-turn) are deeply buried in the hydrophobic phase, whereas the βII-turn is closer to the interface (Figure 4b and c). The local environment has a direct impact on the stability of the β-turns, as becomes visible in Figure 5. Both the hydrogen bonds of the βII′-turn (Ser^6:O–Arg^9:HN) and the cross-link between the amide hydrogen of Gly^4 and the carbonyl oxygen of D-Tic^7 indicate a stabilizing influence of the apolar CCl_4 phase

(46) Kopple, K. D.; Ohnishk, M.; Go, A. *J. Am. Chem. Soc.* **1969**, *91*, 4264–4272.
(47) Kessler, H.; Bats, J. W.; Griesinger, C.; Knoll, S.; Will, M.; Wagner, K. *J. Am. Chem. Soc.* **1988**, *110*, 1033–1049.
(48) Smith, J. A.; Pease, L. G. *CRC Crit. Rev. Biochem.* **1980**, *8*, 315–399.
(49) Rose, G. D.; Gierasch, L. M.; Smith, *J. A. Adv. Protein Chem.* **1985**, *37*, 1–109.

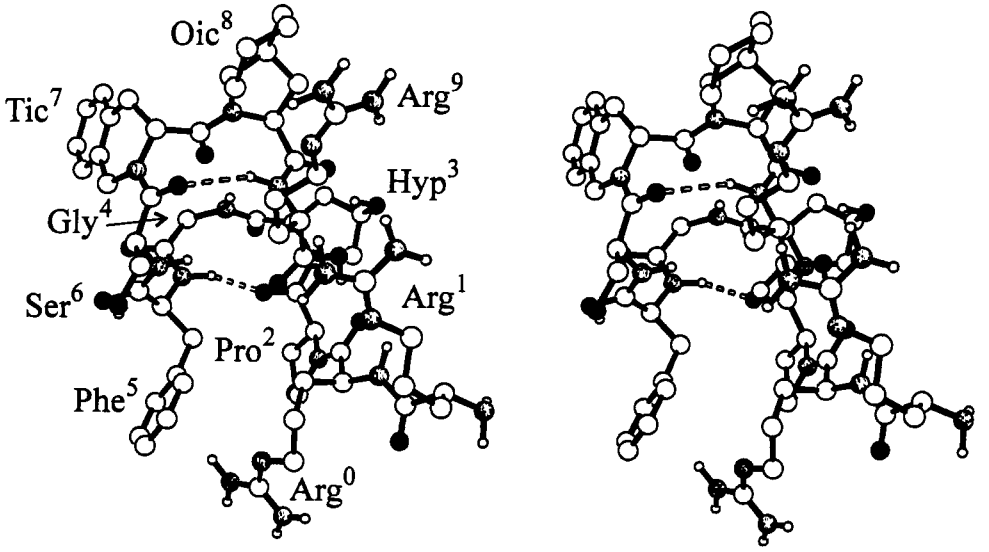

Figure 2. Stereoview of the averaged and energy-minimized conformation of Hoe 140. Apolar hydrogens have been omitted for the sake of clarity. Hydrogen bonds within both β-turns have been indicated by dashed lines.

Table 3. Backbone Dihedral Angles of the Averaged and Energy-Minimized Structure of Hoe 140

	D-Arg^0	Arg^1	Pro^2	Hyp^3	Gly^4	Thi^5	Ser^6	D-Tic^7	Oic^8	Arg^9
ϕ		−132.1	−62.4	−53.5 (−60)[a]	107.8 (80)[a]	−64.8	−133.6	71.4 (60)[b]	−71.4 (−80)[b]	−80.2
ψ	−131.4	163.4	124.2	124.4 (120)[a]	−28.3 (0)[a]	−49.1	79.6	−132.9 (−120)[b]	−5.7 (0)[b]	
ω	−179.9	175.4	172.1	−155.9	173.7	168.0	−172.1	169.6	−163.7	

[a] Idealized backbone dihedral angles for a βII-turn are in parentheses. [b] Idealized backbone dihedral angles for a βII′-turn are in parentheses.

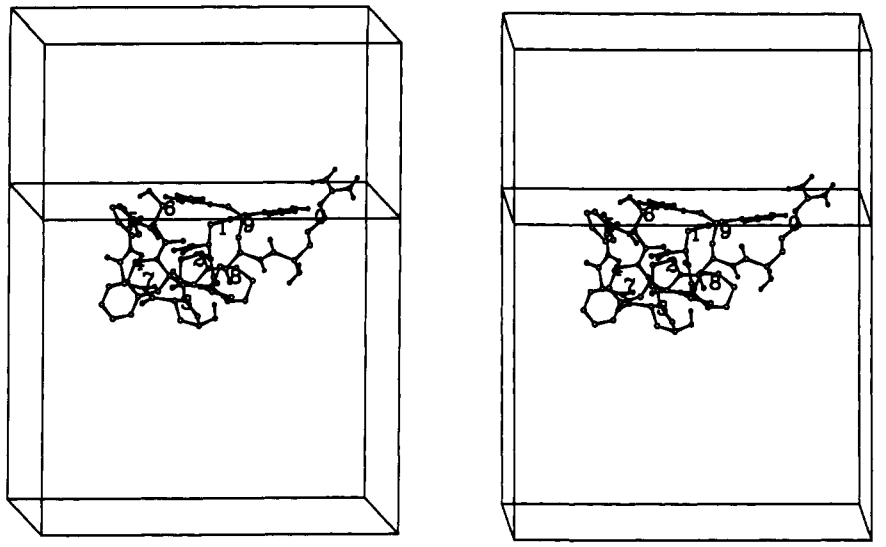

Figure 3. Stereo view of the averaged and energy-minimized conformation of Hoe 140 superimposed on the averaged position in the biphasic H_2O/CCl_4 cell. Apolar hydrogens of the solute and the solvent molecules have been omitted for the sake of clarity. The phase interface has been chosen as the intersection of the H_2O and CCl_4 density profiles.

on the formation of internal hydrogen bonds. In contrast to that, the length of the hydrogen bond of the βII-turn (Pro^2:O–Thi^5:HN) is increasing, as both of the N-terminal arginines tend to immerse into the water phase. As a consequence, the hydrogen bond of the βII-turn is disturbed by the more polar environment. A possible compensating effect of explicit headgroups remains to be explored.

The differing partitioning behavior of the amino acids with hydroxylated side chains is illustrated in Figure 4d. Ser^6 is in the aqueous phase close to the interface mainly involved in hydrogen bonding with water. The hydrogen bond between the serine side chain and the carbonyl oxygen of Thi^5 is only populated by 17% (Figure 6). In contrast to that, the hydroxylic group of Hyp^3 is shielded from the polar phase forming an internal hydrogen bond with the carbonyl oxygen of Oic^8 (population 93%). These observations are further supported by the calculation of radial distribution functions (rdf), $g_{xy}(r)$, which give the probability of finding an atom of type y at a distance r from the atom of type x. The rdfs of the hydroxylic hydrogens of Ser^6 and Hyp^3 relative to water oxygens were calculated (Figure 7) and normalized by dividing the number of water oxygens by the bulk number density. There is one water molecule in the first solvation shell of the serine side chain, as calculated by integration of the rdf up to the first minimum. There is no solvation shell around Hyp^3 in accordance with the calculated probability distribution in the apolar phase.

Unfolding of Hoe 140 in H_2O. As mentioned in the Introduction, NMR measurements in water indicated that the molecule is highly flexible and does not exhibit any conformational preferences (*random coli*). In order to examine the reasons for

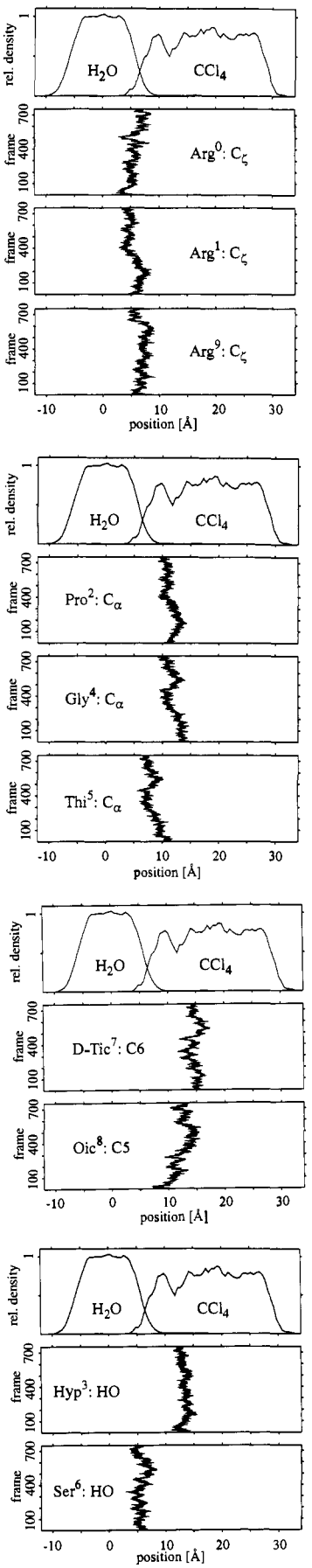

Figure 4. Probability distribution and time course of the *y*-coordinates of selected atoms of Hoe 140 (uncharged) in reference to the density profile of H_2O/CCl_4. During the MD production period 750 snapshots ("frames") have been sampled for 150 ps every 200 fs (see Methods).

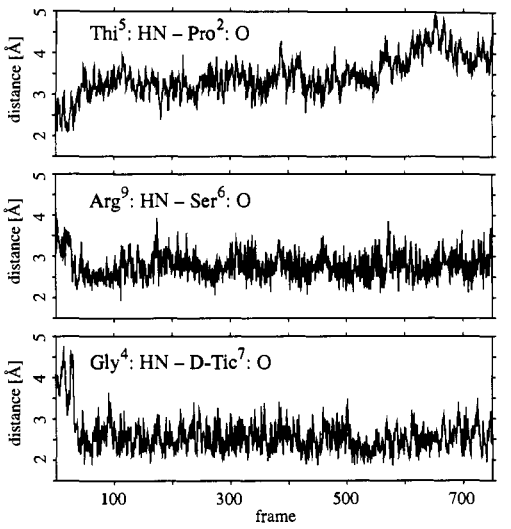

Figure 5. Distances between selected atoms of Hoe 140 (uncharged) monitored over the complete 150-ps trajectory. During the MD production run 750 snapshots ("frames") have been sampled for 150 ps every 200 fs.

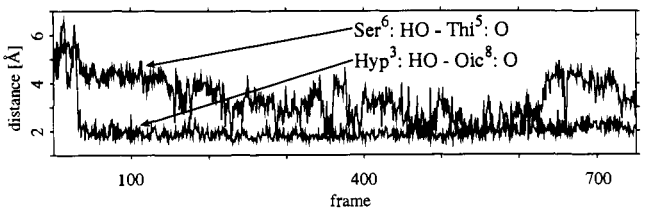

Figure 6. Distances between the hydroxylic hydrogens of Hyp^3 and Ser^6 and selected carbonyl oxygens monitored over the complete 150-ps trajectory (Hoe 140 uncharged). During the MD production period 750 snapshots ("frames") have been sampled for 150 ps every 200 fs.

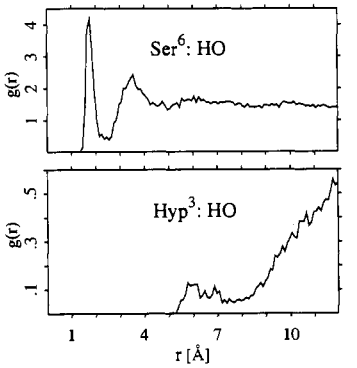

Figure 7. Radial distribution functions of the hydroxylic hydrogens of Hyp^3 and Ser^6 with water oxygens (identical conditions as in Figure 5).

this behavior in water on the atomic level, the averaged and energy-minimized conformation was placed into a H_2O-simulation cell with all ionizable groups treated as charged according to the pH of the NMR measurements. Because of limited CPU time (as mentioned, one iteration of the water simulation took about 1.2 s on a Cray YMP), the production period of the MD simulation could only be performed for a total of 50 ps. For the same reason counterions were not included, as the size of the computational cell would have to be significantly increased to assure sufficient solvation of all charged sites. As can be seen in Figure 8 from the time-resolved distance plots between the amide hydrogen in position $i + 3$ and the carbonyl oxygen in position i of the original β-turns, there is a strong tendency for the peptide to unfold even during the application of the NMR-derived distance restraints. This conformational instability is initialized by the formation of solvation spheres around the guanidino moieties of Arg^0 and Arg^1, which immediately causes the βII-turn, comprising residues 2–5,

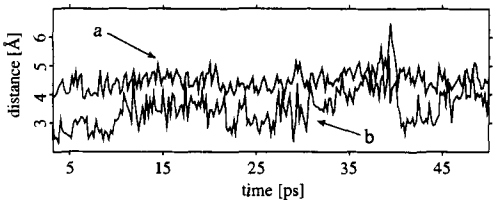

Figure 8. Distances between the amide hydrogens in position $i + 3$ and the carbonyl oxygens in position i of both β-turns (a, Pro²:O–Thi⁵:HN (βII); b, Ser⁶:O–Arg⁹:HN (βII')) of previously refined Hoe 140. The simulation was performed with fully charged Hoe 140 in pure water.

to be disrupted. A similar behavior can be observed for the C-terminal βII'-turn (residues 6–9). As this turn only contains one amino acid with a charged, solvated side chain (Arg^9), the mean value of the corresponding distance between the amide hydrogen and the carbonyl oxygen is lower than that for the βII-turn. The secondary-structure elements established during the biphasic structure refinement appear to be unstable in water in accordance with the NMR results.

Summarizing the results obtained, the folding of the molecule results in a separation of hydrophilic and lipophilic side chains which are exposed to the polar and apolar phase, respectively. As no preferred conformation could be detected by NMR measurements in water, the overall conformation is energetically stabilized by the micellar environment. From a computational point of view, this effect is driven by the largely differing polarities of the two phases ($\epsilon_{293\ K}[CCl_4] = 2.2$; $\epsilon_{298\ K}[H_2O] = 78.5$).[50] Within a biphasic environment, the Coulombic interactions of polar or charged side-chain functionalities with the aqueous phase are, due to the high number density of H_2O, much more favorable than electrostatic contacts with the peptide bonds of the backbone, which avoids a coiling of the peptide. The apolar phase supports the formation of internal hydrogen bonds, enhancing secondary-structure elements, and at the same time prevents water from inserting into these hydrogen bonds. The orientation of an amphiphilic peptide at a phase interface can be rationalized by considering the disturbance of the hydrogen-bonding network induced by apolar residues in the H_2O phase. The phase preference of lipophilic residues for the CCl_4 phase minimizes the loss of Coulombic energy in the aqueous phase and optimizes the van der Waals energy in the apolar phase.

Reorientation of Hoe 140 in H_2O/CCl_4. The structure refinement of Hoe 140 in the biphasic simulation cell was performed by assuming a "chemically reasonable" starting orientation with the three arginine side chains positioned in the aqueous phase. In order to explore different orientations and to account for the simulation conditions that govern the phase preference of a solute, the previously averaged and energy-minimized Hoe 140 was positioned within a simulation cell of increased size with the peptide being completely embedded in the apolar phase.

During preliminary simulations to explore reorientational phenomena of Hoe 140, the effects of charge and NOE restraints were examined. When the complete molecule was treated as uncharged, only a slight drift toward the H_2O phase could be observed within 500 ps (no restraints applied). The electrostatic gradient between the three polar but uncharged arginine side chains and the two hydroxylated amino acids situated in the lipophilic part of the peptide is not sufficient to provide for a strong reorientational driving force.

An analogous procedure with all the arginine side chains and the termini treated as charged resulted in a proper reorientation within less than 100 ps, and all the three guanidino moieties were exposed to the H_2O phase. But during this process the secondary-structure elements were disrupted and large violations of the NMR-derived restraints were observed. This simulation was repeated applying NOE restraints with a maximum force of 1000 kcal $Å^{-1}$ mol^{-1}, leading to an almost static position of the peptide in the simulation cell. The reason for this surprising result is the following: the peptide is not a rigid body; a tumbling motion toward the aqueous phase necessitates structural fluctuations, which are canceled by the restoring forces of the applied restraints. Therefore, the dynamics is reduced to such a degree that a reorientation cannot take place within the relatively short time span. An alternative approach for taking into account the flexibility of the peptide would have been the application of time-dependent distance constraints or ensemble averaging. However, because of the low number of NOEs and the lack of J coupling restraints, a new simulation protocol was devised employing charged groups and a scheme for differently weighting the NOEs determining the shape and the fine structure of the molecule. The aim of this protocol was to maintain the structural integrity and at the same time not to impair the preference of the charged sites for the aqueous phase.

After the averaged and energy-minimized peptide was positioned well within the CCl_4 phase, the system was energy-minimized using the same procedure as in the biphasic structure refinement. For the subsequent MD simulation the restraints were divided into two sets. The first set consisted of the two NOEs involving $Oic^8{}_{H\alpha}$–$Gly^4{}_{NH}$ and $Thi^5{}_{NH}$–$Gly^4{}_{NH}$ and two generic distance restraints between the carbonyl oxygen and amide hydrogen of the amino acids in positions i and $i + 3$ of both β-turns. The second set contained the remaining restraints, whose force constants were scaled with a factor of 0.1. The simulation was carried out for 200 ps at a temperature of 300 K and a pressure of 1.0 bar. Another 400 ps of free MD followed, concluded by a short 50-ps run applying equally weighted restraints.

The reorientational process is illustrated in Figure 9. During the initial 200 ps the electrostatic attraction between the charged arginine side chains and the water phase caused the peptide to drift toward the polar phase until it docked with Arg^9 to the H_2O phase. The unscaled set of restraints maintained the overall topology, whereas the remaining NOE restraints with the reduced force constants exerted restoring forces to structural disruptions caused by the reorientation and, thereby, slowed down the diffusional motion. The subsequent simulation period of 400 ps without restraints allowed the peptide to turn around and to immerse all the charged side chains into the polar phase. The final 50-ps trajectory yielded, after averaging and energy-minimizing, the conformation described above.

The reorientational process can also be illustrated by following the time course of two diagnostic atoms within the coordinate system of the density profile of H_2O/CCl_4. As can be seen in Figure 10, atom C5 of amino acid Oic^8 moves toward the polar phase, which corresponds to the drifting of the peptide in the direction of the interface. The atom C_ζ of amino acid Arg^1 covers a considerably greater distance, which can be rationalized by a slow rotation of the molecule superimposed on the diffusional motion. This rotation exposes the side chain of Arg^1, formerly buried within CCl_4, to the polar phase.

Concerning the orientation of Hoe 140 at the phase interface, a slightly different result was obtained when compared to that of the simulation without charged groups. Whereas in the latter calculation Ser^6 was exposed to the water phase and the hydroxylic group of Hyp^3 was involved in an internal hydrogen bond to the carbonyl oxygen of Oic^8, the situation was reversed in the simulation with ionic groups. As can be seen from the distance plot of the hydrogen bond between Ser^6 and the carbonyl oxygen of $Phe(Thi)^5$ and the respective radial distribution functions of the hydroxylic hydrogens of both Ser^6 and Hyp^3 with water (Figure 11), both OH groups were buried in the CCl_4 phase, forming no solvation spheres for the initial 400 ps. During the interval 400–600 ps, Hyp^3 became attached to the aqueous phase (the

(50) Weast, R. C.; Ed.; *CRC Handbook of Chemistry and Physics*; CRC Press: Boca Raton, FL, 1985.

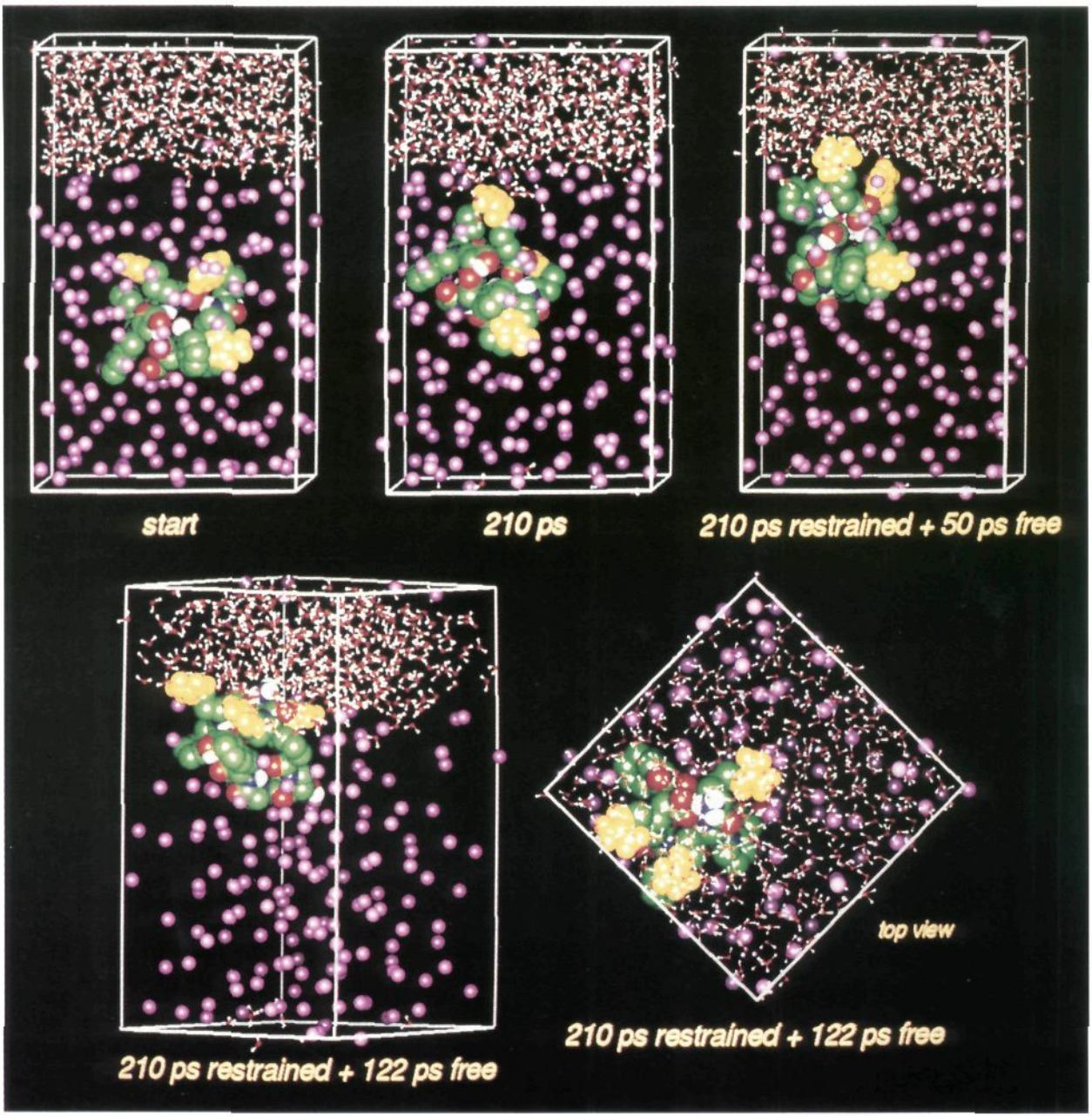

Figure 9. Reorientation of charged Hoe 140 in H_2O/CCl_4 (*united atom* approach for CCl_4). The van der Waals radii have been scaled differently, and the guanidino moieties have been depicted in yellow for the sake of clarity.

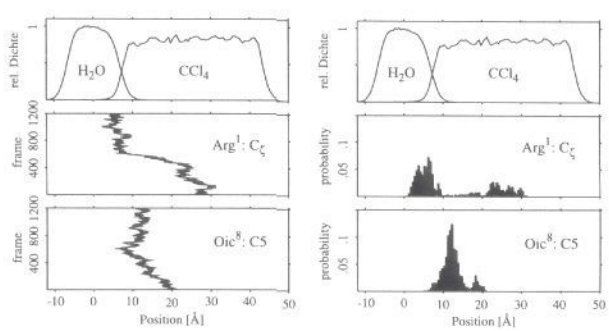

Figure 10. Time course and probability distribution of the *y*-coordinates of diagnostic atoms of Hoe 140 (charged) in reference to the density profile of CCl_4/H_2O. During the MD production period 1200 snapshots ("frames") have been sampled for 600 ps every 500 fs.

integration of the first peak of the rdf yields one water molecule), whereas Ser[6] was still engaged in an internal hydrogen bond.

The different solvation behavior of Ser[6] and Hyp[3] employing different charge models for Hoe 140 can be explained as follows. First of all, the ionic groups used in the second simulation have a greater affinity for the H_2O phase than the polar but uncharged functional groups of the first simulation, leading to a greater depth of penetration. If a computationally expensive explicit membrane model was employed, the headgroups might act as a buffer zone and reduce the depth of penetration into the water phase. Secondly, there are neither experimental restraints nor additional terms in the force field to define the orientation, so the observed difference in selective solvation represents two low-energy orientations with an energy barrier too high to be cross during the simulation period. In this context, MD within a biphasic system is an interesting tool to scan different orientational minima by taking into account the conformational flexibility of the substrate.

In this context, we want to emphasize that we are well aware that the time scale of MD simulations is much too small to

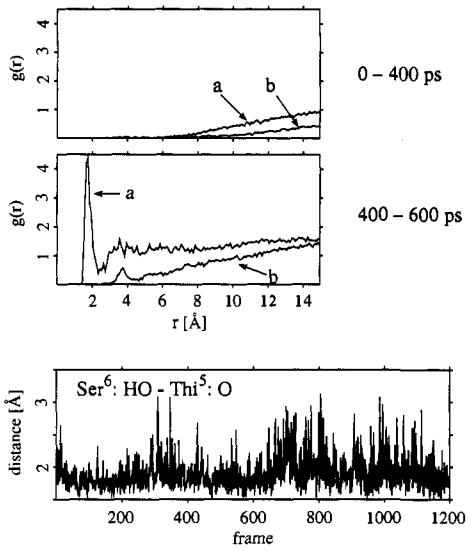

Figure 11. Radial distribution functions $g(r)$ of hydroxylic hydrogens of (a) Hyp[3] and (b) Ser[6] with water oxygens averaged over the initial 400 ps and the final 200 ps of the 600-ps production period (Hoe 140 charged). Bottom: Time-resolved distance plot covering the total simulation period of 600 ps between the hydroxylic hydrogen of Ser[6] and the carbonyl oxygen of Phe(Thi)[5].

calculate the distribution coefficient of the solute between the two phases. As no experimental restraints are applied for the orientation and the depth of intrusion, the molecule may well rest in a local minimum similar to local minima in the conformational space of flexible molecules. However, the calculations are well able to elucidate the behavior of amphiphilic molecules at the interface.

Conclusion

Applying a combined approach of NMR measurements in SDS micelles and molecular dynamics simulations in a novel biphasic (H_2O/CCl_4) membrane mimetic, the conformation of the bradykinin antagonist Hoe 140 and its orientation at the phase interface were determined. The secondary-structure elements were not established during the in vacuo MD simulation with NMR-derived distance restraints but only formed within the H_2O/CCl_4 simulation cell. Furthermore, the calculated conformation proved to be unstable in water, in accordance with experimental results. The structure-enhancing effect of the micellar environment as observed by NMR spectroscopy and validated by MD simulations is assumed to be correlated with the bioactive conformation under physiological conditions. In the extracellular aqueous phase, BK adopts a random structure because of the lack of conformational restraints. The recognition of BK by its membrane-bound G-protein coupled receptor (GPCR) might be facilitated by the biological target cell membrane which induces the orientation and conformation corresponding to the structural and stereochemical requirements of the binding site.

NMR measurements in membrane-like environments are hampered by broad line widths because of long correlation times and by frequent signal overlap of the substrate and the micelle- or membrane-forming agent. Consequently, the quantity and the quality of the NOEs and scalar coupling constants are often not sufficient for a distance geometry algorithm, which solely rests upon interatomic distances. Therefore, MD simulations employing a physical force field within a biphasic computational cell, triggering the separation of polar and apolar regions as often observed in membrane-like surroundings, are an interesting alternative. As described above, the biphasic environment promoted the formation of secondary-structure elements, whereas an in vacuo or pure solvent simulation yielded no reasonable interpretation of NMR data.

Employing a fully charged model for the peptide, a proper reorientation could be achieved starting from an arbitrary location within the apolar phase of the H_2O/CCl_4 cell. Critical issues, which had not been dealt with because of limited computational resources, are how counterions or the headgroups of an explicit membrane/micelles influence the depth of penetration of charged groups into the polar phase. Nevertheless, the reorientation demonstrates that the biphasic simulation cell is able to realistically describe the correct phase preference.

In contrast to the calculation of partition coefficients from quantitative structure activity relationships (QSAR), the introduced model takes into account the conformational flexibility of the substrate. Thus, this recently introduced membrane mimetic for use in MD simulations proved to be an effective and computationally efficient means for the structural and orientational characterization of amphiphilic peptides in membrane-like surroundings.

Acknowledgment. This study was supported by the SFB 266 of the Deutsche Forschungsgemeinschaft and the Fonds der Chemischen Industrie.